

Mechanical Design, Structural Analysis, and Static Fire Testing of a Jet Vanes System for Thrust Vectoring

Kush Bandi*, Pritham Sathish†, Alex Zangara‡
Georgia Institute of Technology, Atlanta, GA, 30332

Jet vanes are a method for active control in rocket propulsion systems that involve actuating control surfaces (vanes) inside exhaust flow. By redirecting the flow, these vanes induce control forces on the rocket. This work addresses the key challenges of integrating a jet vane structural system with commercial-off-the-shelf (COTS) solid rocket motors, particularly in withstanding extreme thermal and erosive conditions, retaining structural integrity under high loads, and minimizing mechanical packaging within space constraints of COTS airframes. This study presents the design of a jet vane assembly (JVA) capable of withstanding thrust forces up to 2.2 kN while maintaining precise vane control. The initial assembly featured a sandwich-design structural assembly for its low weight, a two-stage drivetrain to distance vane-driving actuators from motor exhaust, and tungsten-copper control vanes for their manufacturability. This design was structurally verified by finite element analyses (FEA), and initial static fire results validated the structural assembly and control vane drivetrain. However, results also revealed excessive erosion of control vanes and unprecedented exhaust heating. Consequently, the current iteration of the JVA employs a pure tungsten control vane for its superior hardness, a thermal protection system to further isolate actuators from exhaust backflow exposure, and structural and drivetrain assemblies identical to the first iteration, all of which will be verified by an upcoming final static fire before rocket integration and launch. This work establishes that a jet vanes active control system can be developed within the constraints of collegiate rocketry environments.

I. Nomenclature

a	=	overhung length
E	=	elastic modulus
F	=	gear tooth face width
I	=	area moment of inertia
l	=	supported length
P_{app}	=	applied load
P_d	=	diametral pitch
W_t	=	tangential load
y_{max}	=	maximum distance from beam neutral axis
Y	=	Lewis form factor
δ_{max}	=	maximum beam deflection
σ	=	stress
$\sigma_{b,\text{max}}$	=	maximum beam stress
$\sigma_{t,\text{max}}$	=	maximum gear tooth stress
σ_{allow}	=	allowable stress

II. Introduction & Motivation

THURST vector control (TVC) is a critical technology in rocketry, enabling active control of vehicles through the manipulation of engine exhaust to generate control forces. Distinct from aerodynamic control surfaces, which

*Structures Co-Lead, GT Ramblin' Rocket Club, Aerospace Engineering, AIAA Undergraduate Student Member 1603558

†Structures Co-Lead, GT Ramblin' Rocket Club, Aerospace Engineering, AIAA Undergraduate Student Member 1536656

‡Structures Member, GT Ramblin' Rocket Club, Aerospace Engineering, AIAA Undergraduate Student Member 1811146

become less effective at high altitudes and low velocities, TVC provides control authority throughout all phases of powered flight. There are three primary methods of TVC: gimbale nozzles, secondary fluid injection, and mechanical flow obstruction. Among these, jet vane thrust vector control (JVTVC) offers an effective solution for medium-scale solid rocket motors, where gimbale nozzles face challenges related to space constraints and mechanical complexity, and fluid injection requires additional tanks and plumbing. JVTVC employs small, high-temperature-resistant jet vanes precisely positioned aft of the motor nozzle to directly perturb exhaust flow, producing pitch, yaw, and roll control forces.

The Guidance, Navigation, and Control (GNC) Team within Georgia Institute of Technology's Ramblin' Rocket Club (RRC) has developed a JVTVC system as part of its effort to design and build an actively stabilized solid-propellant rocket. This work presents the mechanical design and development process of the jet vane assembly (JVA). The design was subjected to a multi-phase iterative process involving system requirement definitions, subsystem breakdown, structural analysis, and validation through static fire tests. The culmination of this process is the current iteration of the JVA in Fig. 1, partially validated by a first static fire and primed for a second static fire. This assembly features a sandwich-design structural assembly, a two-stage drivetrain, pure tungsten control vanes, and a two-part thermal protection system (TPS). This paper details the development of the JVA, highlighting the engineering and design decisions that shape its present configuration.

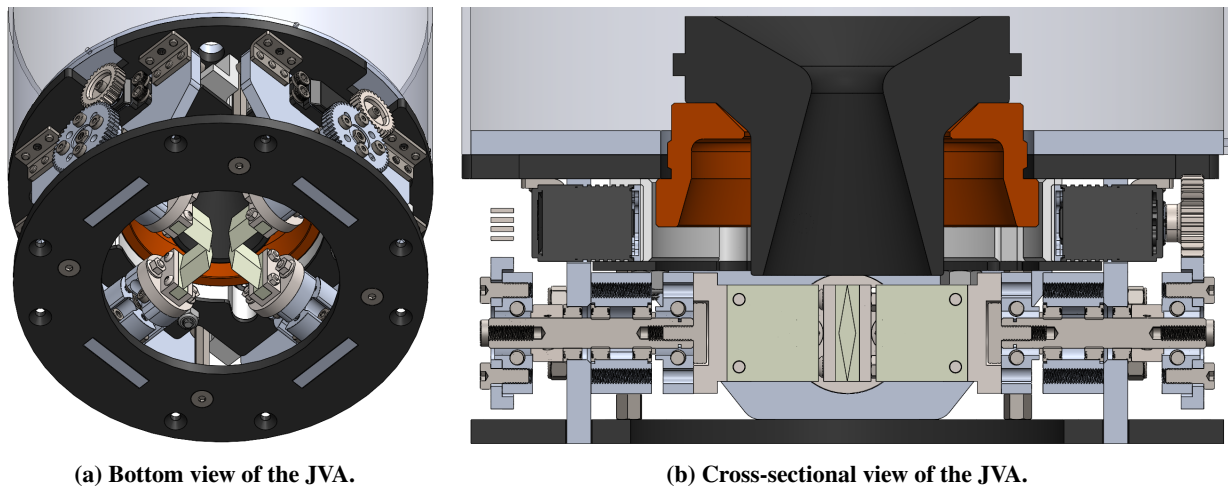


Fig. 1 Developed iteration of the JVA.

III. System Requirements

The critical determining factors of requirements were team-allocated budget, GNC Controls and Simulation Team constraints, available manufacturing techniques, and the proposed one-year timeline of static fire testing and rocket development. Based on these factors, the following requirements were identified to regulate development of the JVA:

- 1) The JVA shall retain complete mechanism functionality during and after the burn of the AeroTech N1000W solid motor.
- 2) The JVA shall retain factors of safety (FoS) of at least 1.5 on all components critical to the structure and stability of the jet vanes.
- 3) The JVA shall be completely housed within COTS fiberglass rocket airframes.
- 4) The JVA shall interface custom-machined structures with COTS actuation and mechanism components.
- 5) The JVA shall utilize a jet vane geometry developed by the Simulations Team.
- 6) The JVA actuator shall satisfy torque requirements from the Simulations Team and feedback requirements from the Controls Team.
- 7) The JVA jet vanes leading edge shall be mounted 0.1 inches from the exit plane of the nozzle.
- 8) The JVA shall be designed for fast and repeatable manufacturing cycles between static fires and rocket integration.
- 9) The JVA shall comply with the Tripoli Rocketry Association (TRA) safety code with regard to the usage of ferrous components.

With established requirements on design, performance, and manufacturing, the development process transitioned into the system subassembly design and analysis phase.

IV. Structural Assembly

The structural assembly refers to the larger mechanical components responsible for housing and integrating the jet vane drivetrain assembly. The objective of the structural assembly was to route axial loads to the rocket airframe while providing a framework for the jet vane actuation system. The selected structural assembly architecture follows a “sandwich” design. This architecture, outlined in Fig. 2, was selected among other potential designs due to its high strength-to-weight ratio and ease-of-manufacturing using 2D operations such as waterjet cutting or 2-axis CNC milling. Additionally, this architecture provides flexibility in the vertical mounting location of the jet vanes and actuators, satisfying Requirement 7.

The *Flange Plate* serves as the primary interface and load-transferring mechanism between the JVA actuation system and the rocket airframe. The flange of the aft ring makes flush contact with the flange plate at its inner diameter, and the airframe makes flush contact with the flange plate at its outer diameter, creating a load path from the aft ring to the airframe.

The *Actuator Mounting Plate* provides a flexible mounting location for the actuators and jet vanes. These plates explicitly position actuators behind the exit plane of the nozzle and jet vanes 0.1 inches aft of the nozzle. The actuator mounting plates are secured to the top plate using angle brackets and fixed above and below by tab-cutout interfaces with the flange and bottom plates.

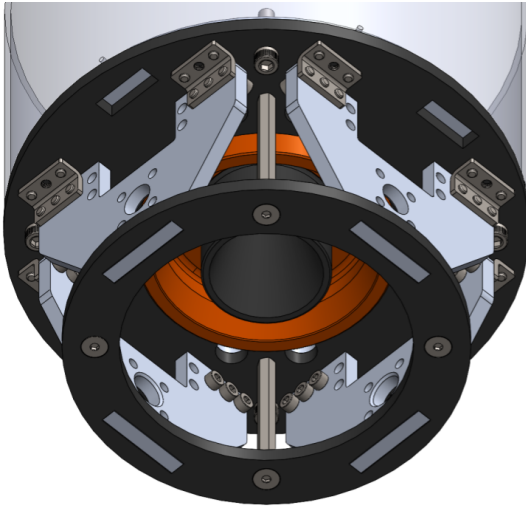


Fig. 3 Bottom view of the JVA structural assembly.

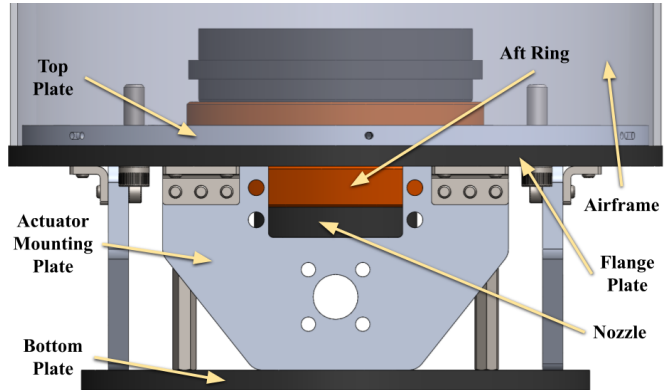


Fig. 2 Side view of the JVA structural assembly.

The *Top Plate* is designed to facilitate the integration of the JVA into static fire and rocket architectures. To achieve this, it contains axially threaded holes on its face and can be permanently secured onto the airframe before other assembly. During rocket integration, the rest of the JVA can be assembled separately and then swiftly secured by bolting the flange plate into the facial holes of the top plate. Furthermore, the top plate is recessed within the airframe above the flange plate, forcing axial loads to be directed through the flange plate and transferred to the airframe, avoiding the top plate and making it a low-load-bearing component.

The *Bottom Plate* completes the sandwich using tab-cutout interfaces with the actuator mounting plates. When the bottom plate is secured to the vertical standoffs, it constrains the actuator mounting plates through the tab-cutout interface. This constraint increases the bending rigidity of the actuator mounting plates, which is verified in Section VI.B. This structural assembly design provides an initial foundation for drivetrain assembly development, and material determination for all plates in the structural assembly is outlined in Section VI.A.

V. Drivetrain Assembly

The drivetrain assembly is responsible for the transfer of rotational control from the actuator to the jet vanes. It operates according to the requirements of the Controls and Simulations Teams. The drivetrain assembly implements a two-stage geared architecture, selected due to its ability to distance actuators from high-temperature regions near the exit plane of the nozzle.

A. Drivetrain Architecture & COTS Integration

The first stage consists of the COTS actuator and output gear. The chosen gear is a steel 30-tooth gear, matching the actuator output spline. The material of this gear provides a yield stress large enough to retain a sufficient FoS during operating conditions, as established in Section V.C, while the matching spline allows for direct interface with the actuator. The gear is secured to the actuator with a bolt threading through the actuator spline, and the actuator is then secured to the actuator mounting plate with bolts and nuts. This complete first stage is depicted in Fig. 4.

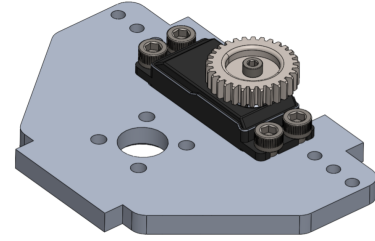


Fig. 4 First stage of the JVA drivetrain.

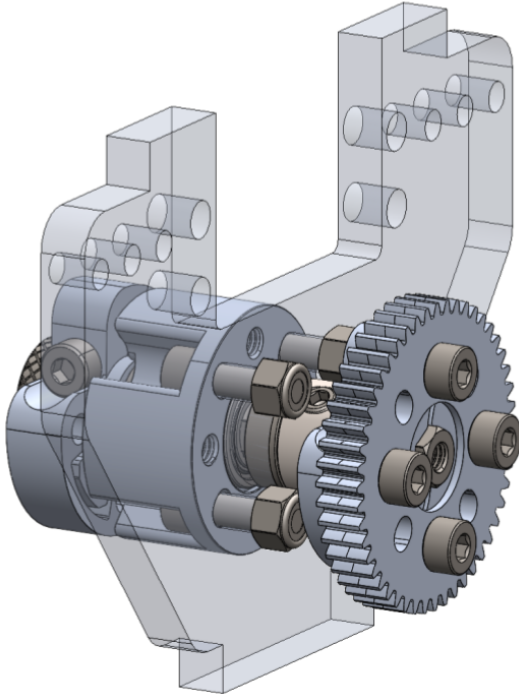


Fig. 5 Second stage of the JVA drivetrain.

The primary portion of the second stage is comprised of the geared power transfer from the first stage, the driving shaft, and the shaft's constraining components. This region of the JVA is where COTS integration is most prominent, with many parts selected from the GoBilda[®] catalog due to its easy integration and well-defined tolerances. The driving shaft was selected as an 8mm Hex Shaft. The geared transfer employs a 48-tooth Hub Mount Spur Gear, and an 8mm Hex Sonic Clamping Hub allows the spur gear to be secured to the driving shaft. An 8mm Hex Collar is placed flush against the clamping hub and prevents slippage of the shaft along its length axis. The collar also has a flush interface with an 8mm Hex Flanged Radial Bearing, which rests in the actuator mounting plate. All components of the primary portion of the second stage are depicted in Fig. 5, with detailed views in Fig. 7a.

On the opposite side of the actuator mounting plate resides the secondary portion of the second stage, consisting of continued driving shaft support, the jet vane interface with the COTS ecosystem, and the jet vane. To provide shaft bending support, an 8mm Dual-Bearing Pillow Block is bolted to the actuator mounting plate. Importantly, the dual internal bearings of the pillow block added to the radial bearing intentionally overconstrain the driving shaft. Though adding friction to rotational movement, the triple-bearing structure adds a third support in between the two contacts of an initially dual-support overhung

beam, reducing tip deflection. A 1mm Shim is placed on the rear bearing of the pillow block to ensure protection of the bearing flange, and another 8mm Hex Sonic Clamping Hub is placed at the end of the shaft, providing mounting holes for custom jet vane support. For redundancy, a thumb screw threads into the end of the shaft to guarantee the clamping hub does not slide off the driving shaft during operation. The secondary portion of the second stage is displayed in Fig. 5, with detailed views in Fig. 7a.

Completing the second stage is the interface between the clamping hub and the jet vane, called the "vane backing," and the jet vane itself. Due to the proximity of these components to the erosive exhaust flow, the driving requirement was the usage of high-melting and high-hardness materials, constraining their design and geometry due to limited manufacturing capabilities. The vane backing was selected to be titanium due to its particularly low thermal conductivity and high specific heat capacity, allowing it to act as a heat sink and resist conduction to the rest of the drivetrain. The vane backing was designed with only two primary features: a circular boss, sized to COTS titanium, and a rectangular boss, to minimize manufacturing operations. The vane backing directly mounts to the clamping hub using its existing mounting holes, and the opposing side employs a slot-key design to mount the jet vane. This mounting feature was selected due to its minimal manufacturing operations but large contact regions, allowing more heat transfer from the jet vane to the vane backing.

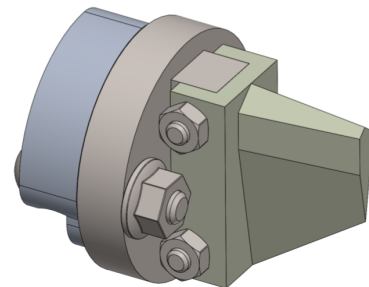


Fig. 6 The jet vane and vane backing.

The jet vane geometry is constrained by the tapered kite-shaped contour provided by the Simulations Team and the 75-25 tungsten-copper material selection due to its high melting point, high thermal conductivity to dissipate heat into the vane backing, and manufacturability [1]. These requirements drive the entire design of the vane itself, with the latter half of the slot-key design featured at the root chord of the vane. The clamping hub, vane backing, and jet vane are fixed together using titanium bolts and nuts due to their high shear strength. The jet vane, vane backing, and clamping hub interfaces are visualized in Fig. 6, and consolidation of both drivetrain stages with the actuator mounting plate is visualized in Fig. 7.

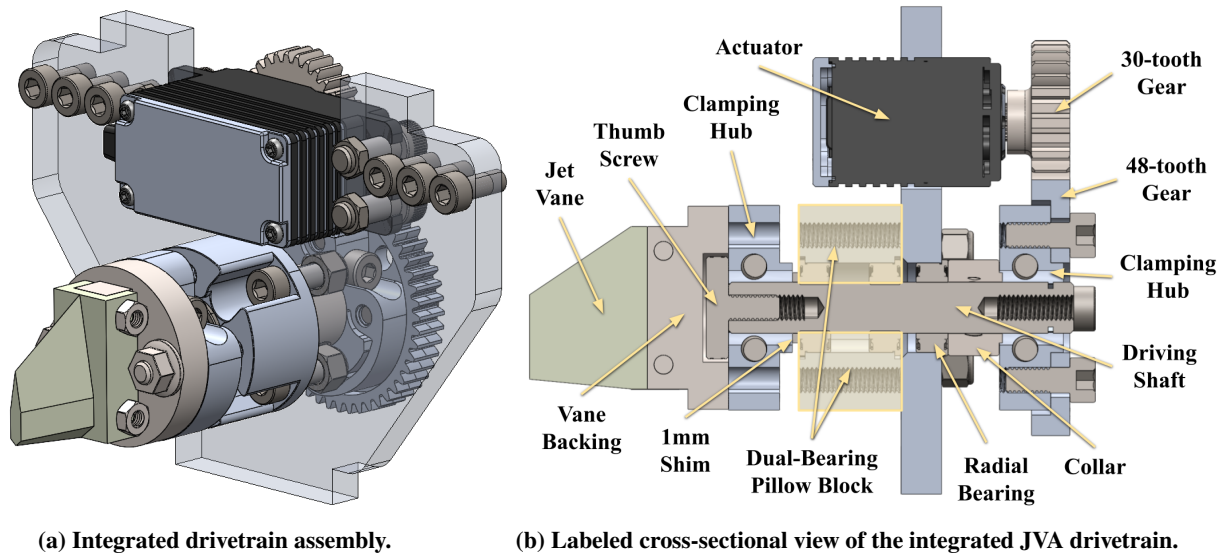


Fig. 7 Integrated drivetrain assembly interfaced with the actuator mounting plate.

B. Actuator Selection

The requirements on actuator selection are necessary torque, rotational range of motion, feedback, and desire of minimal actuator form factor. With the specific jet vane geometry and the flow conditions of the N1000W motor, the Simulations Team expects a maximum applied torque of 0.68 N-m about its point of rotation; even though rotating about its center of pressure, high-speed flow and high angles of attack still result in applied torques that the actuator must withstand. Additionally, the actuator is required to provide positional feedback but does not need to rotate continuously past 360° as jet vanes systems, by design, do not require a full range of motion.

Considering these criteria, the Axon Mini+ [2] servo motor was selected. With operating voltage and gear reduction, this actuator has a torque FoS of 7.61 on the jet vanes' maximum torque from simulations. This servo motor also provides positional feedback in the 60-degree range of jet vane actuation. Furthermore, it retains a smaller form factor than traditional servo motors, contributing to drivetrain assembly compactness.

C. Architecture Feasibility Studies

Preliminary analysis of the drivetrain-powering spur gear teeth stress provides initial feasibility of the drivetrain architecture. As the jet vanes face an applied torque at high rotation angles, initial qualification of the design can be obtained by computing the stress FoS on the teeth of the spur gears. The Lewis Equation, given in Eq. (1), presents a simplified analysis of gear stresses by computing the maximum static stress on the tooth [3]. Assuming the gear tooth to be a flat plate and not experiencing dynamic loads, the maximum static stress is located at the gear tooth root:

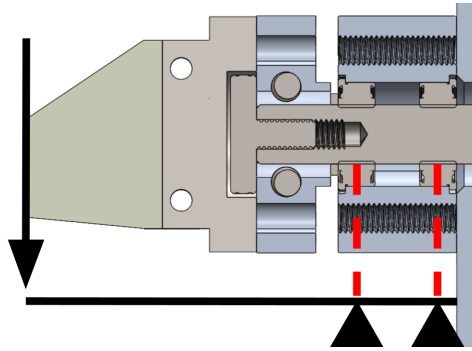
$$\sigma_{t,\max} = \frac{W_t P_d}{FY} \quad (1)$$

Assuming no axial gear tooth loading for a worst-case scenario, the tangential load can be extrapolated by multiplication of the maximum applied torque of 0.68 N-m and gear addendum circle radius, while the pitch diameter and face width are both provided properties of the COTS spur gears. The Lewis form factor was selected as 0.4 based

on the number of teeth and tooth geometry. The FoS was then determined according to Eq. (2).

$$\text{FoS} = \frac{\sigma}{\sigma_{\text{allow}}} \quad (2)$$

Using the computed maximum static stress and the tensile strength of 6061-T6 aluminum [4] (the material of the 48-tooth gear) as the allowable stress, the 48-tooth gear retains a FoS of 6.23. The steel-hardened, zinc-plated 30-tooth gear retains an even higher FoS of 7.77 due to its raised tensile strength [4]. It is also possible to compute gear tooth dynamic stresses, but it is unnecessary due to the slow rotational motion of the drivetrain.



In addition, the initial feasibility of the driving shaft with respect to maximum deflection and stress is determined. The driving shaft is decomposed into two simply-supported beams overhanging one support with a concentrated load at its end, visualized in Fig. 8. The maximum deflection, located at the shaft tip, is given by Eq. (3):

$$\delta_{\text{max}} = \frac{Pa^2}{3EI}(l + a) \quad (3)$$

Additionally, the maximum bending stress in this simplified model is given by Eq. (4):

$$\sigma_{b,\text{max}} = \frac{Py_{\text{max}}a}{I} \quad (4)$$

Fig. 8 Decomposition of the drivetrain into a simply-supported beam model.

Assuming the entire simplified beam model has the properties of the steel 8mm Hex Shaft and applying a concentrated force of 250 N obtained by the Simulations Team, Eq. (3) yields a maximum deflection of 0.2mm, which does not have an impact on the jet vanes' ability to redirect flow. Additionally, applying the result from Eq. (4) with Eq. (2) and using the allowable stress for the shaft material, AISI Type 314 stainless steel [4], the driving shaft retains a stress FoS of 1.9. These two preliminary computations provide a baseline feasibility for the JVA drivetrain, permitting continuation into FEA.

VI. Static Structural Analysis

To increase design fidelity from preliminary computations, the static structural response is analyzed in Ansys FEA on the proposed combined structural and drivetrain assemblies. This analysis informs design decisions and assembly material selection to further guide the JVA development process. The primary steps of the simulation process were model defeaturing, temperature-based material property modification, simulation boundary condition setup, and simulation.

The integrated drivetrain and structural assemblies were defeatured for computational efficiency. All components in the integrated assembly, with the exception of the jet vane itself, were remodeled using only circular, rectangular, or hexagonal features. Moreover, since these simulations and analyses are only interested in the behavior of components near the flow regime, the drivetrain was partly excluded. Only a single vane and respective partial drivetrain are considered, as all four jet 4 vane shaft components were identical. The transformation from the integrated fully featured model to the integrated defeatured model is shown in Fig. 9.

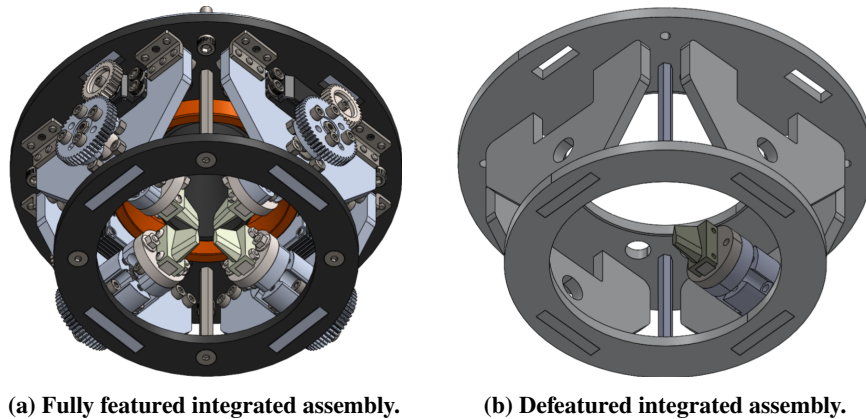


Fig. 9 Defeaturing process of the JVA in preparation of simulations.

Following defeaturing, the elastic moduli of materials were modified in Ansys based on worst-case thermal conditions provided by the Simulations Team. As elastic modulus generally decreases with increased temperature in metals, the deflection and experienced stress are consequently impacted. The jet vane and vane backing are within the flow regime, undergoing significant temperature changes and, consequently, considerable decreases in elastic moduli. From CFD simulations, the maximum temperature of each component is extracted, and the entire component is assumed to be that temperature as a worst-case analysis. Then, the elastic moduli are modified to reflect the temperature. The vane backing is expected to reach 1100°C, resulting in a reduced elastic modulus of 45.1 GPa [5]. The jet vane is expected to reach 1600°C, but due to limited research on high-temperature properties of the tungsten-copper alloy, its elastic modulus is approximated to be 75% of pure tungsten’s moduli at 1670°C, 263 GPa [6].

Subsequently, boundary value and initial value conditions were applied to reflect airframe integration conditions. As mentioned previously, the flange plate is bolted to the top plate during JVA integration, and therefore, the bolt interface is treated as a fixed support. In addition, the flange plate is axially constrained at its inner diameter by the flange plate; the flush contact region between these two components is also treated as fixed. The applied load to the vane is simplified to a pressure load of 250 N on the leading faces of the jet vane — the highest load experienced by the jet vane at its maximum angle of attack.

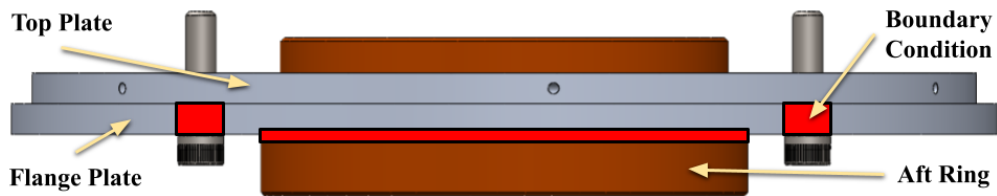


Fig. 10 Boundary condition application to the flange plate.

With these boundary and initial conditions, a preliminary simulation is run with all structural assembly materials initially selected as 6061-T6 aluminum to obtain qualitative results before full material trade studies; these results are shown in Fig. 11. The maximum system deflection occurs at the jet vane leading edge, while the maximum system equivalent stress occurs on the actuator mounting plate, with smaller stress concentrations found in the flange plate and bottom plate near edges and mounting holes.

A. Structural Assembly Material Selection

After a preliminary qualitative analysis, the material selection process began. Related to Requirement 9, the TRA safety code states general avoidance of large ferrous materials for rocket components near the exhaust, immediately removing steel from being a material candidate. Additionally, the JVA aims to minimize jet vane deflection whilst lowering system weight to reduce the bottom-heaviness of the vehicle, leaving aluminum alloys and G10 Fiberglass as the only available and machinable materials feasible in the budget of the GNC project.

The only forced material selection is that of the top plate; it is required to be aluminum over G10 due to its radial and axial threaded holes, which are infeasible to manufacture in G10 due to its low ductility. However, the flange plate, actuator mounting plate, and bottom plate all have the option of G10 or aluminum, yielding eight possible material selection combinations. Static structural simulations were run for each combination; maximum

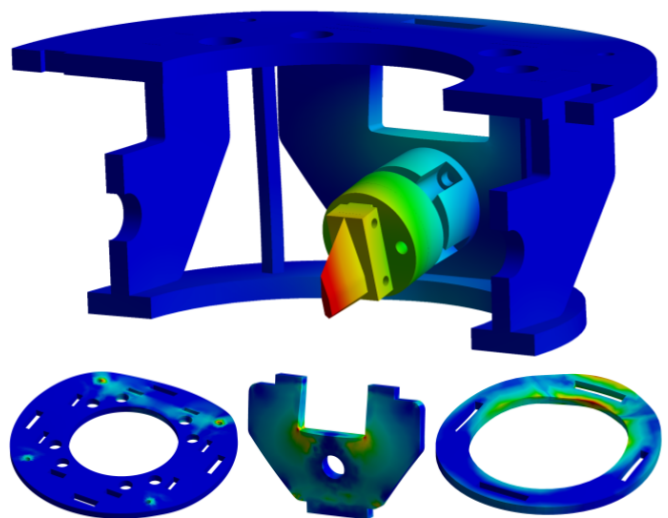


Fig. 11 Qualitative results of JVA total deformation and equivalent plate stress.

vane leading edge deflection and structural plate maximum equivalent stresses were extracted from Ansys. The stress FoS for each plate was also computed using Eq. (2). Table 1 summarizes these response quantities:

Table 1 Vane Leading Edge Deflection, Structural Assembly Stresses, and Factors of Safety with Varying Plate Material Selection

Bottom Plate Material	Actuator Plate Material	Flange Plate Material	Jet Vane Leading Edge Deflection (mm)	Max Equivalent Stress (MPa)			Factor of Safety			Net Weight (lbs)
				Bottom Plate	Actuator Plate	Flange Plate	Bottom Plate	Actuator Plate	Flange Plate	
ALU	ALU	ALU	0.130	5.793	25.108	9.948	41.6023	9.599	24.226	2.70
ALU	ALU	G10	0.139	6.887	26.523	8.301	34.995	9.087	5.650	2.42
ALU	G10	ALU	0.221	8.699	21.334	11.966	27.704	2.198	20.140	2.45
ALU	G10	G10	0.238	8.612	22.040	10.661	27.982	2.128	4.399	2.17
G10	ALU	ALU	0.149	3.940	27.973	9.416	11.905	8.6155	25.595	2.59
G10	ALU	G10	0.163	3.972	33.663	8.584	11.807	7.159	5.464	2.31
G10	G10	ALU	0.247	6.209	22.872	11.627	7.553	2.051	20.728	2.34
G10	G10	G10	0.264	6.022	23.841	10.933	7.788	1.967	4.290	2.06

The results of this trade study narrow down the bottom plate, actuator mounting plate, and flange plate material selection. Leading edge vane deflection is shown to be primarily a function of actuator plate material, nearly doubling when selected to be G10. Moreover, when the actuator plate is G10, its stress FoS is significantly lower than when selected to be aluminum, with little weight benefits, eliminating configurations 3, 4, 7, and 8. Inspecting the impacts of flange plate material selection, the leading edge vane deflection is not impacted by material variance; since the flange plate retains a high FoS and significantly decreases weight when G10, it is selected as such, eliminating configurations 1 and 5. Left with arrangements 2 and 6, option 6 is chosen due to its lighter weight and FoS retention. Thus, the design proceeds with configuration 6, where an aluminum actuator mounting plate is sandwiched between G10 flange and bottom plates — a material arrangement providing the best tradeoff between vane leading edge deflection, plate stress FoS, and JVA weight.

B. Verification of Bottom Plate Inclusion

In addition to plate material determination, simulations also confirm the necessity of the bottom plate; observation of leading edge vane deflection and actuator mounting plate maximum equivalent stress reveals that the bottom plate is providing structural support as desired.

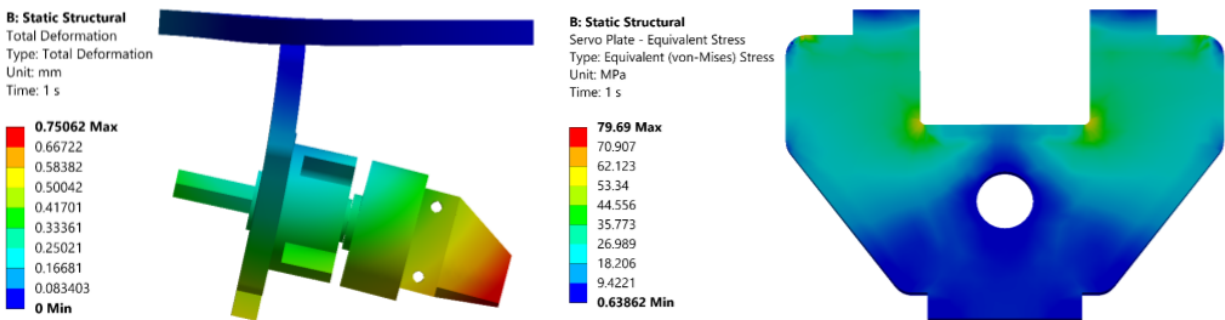


Fig. 12 JVA total deformation and actuator mounting plate equivalent stress excluding the bottom plate.

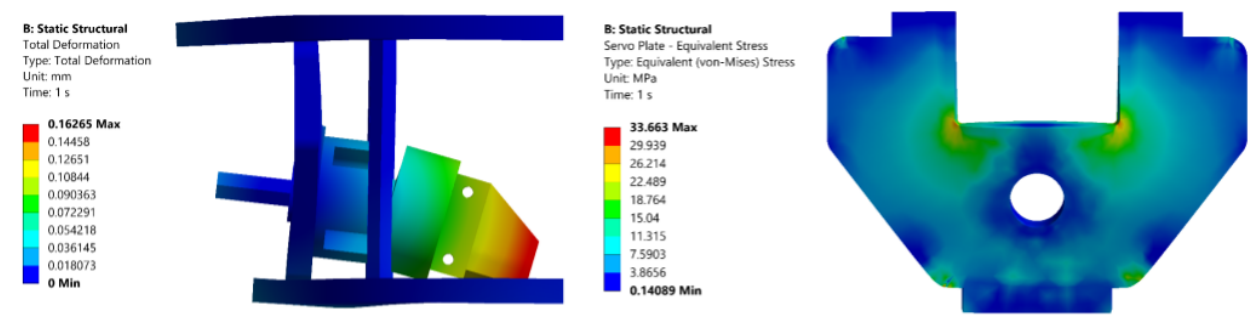
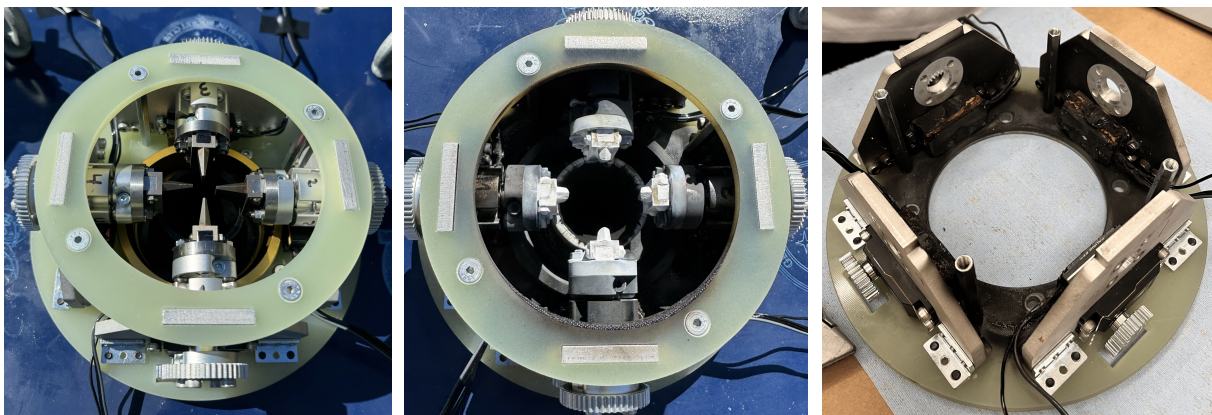


Fig. 13 JVA total deformation and actuator mounting plate equivalent stress including the bottom plate.

The system total deformation and actuator mounting plate equivalent stress both experience sharp increases when the JVA is devoid of the bottom plate, as exhibited in Fig. 12. The bottom plate is shown to absorb and distribute energy among the system at the cost of extra weight, confirmed in Fig. 13, validating its inclusion in the JVA.

VII. Static Fire Results & Post-Static Fire Improvements

The JVA was unable to demonstrate effective thrust vectoring during the static fire as the jet vanes fully eroded due to the motor's aluminum oxide particulate exhaust in under 3 seconds of the full 13-second burn. As the machinability was prioritized and the melting temperature was improperly understood during the initial material selection, the decision of tungsten-copper was ill-informed and did not emphasize the impact of material hardness on erosion. Fig. 14a and Fig. 14b showcase pictures of the JVA before and after the static fire. Though the jet vanes eroded, the rest of the structural and drivetrain assemblies ultimately withstood the motor burn. Structurally, the only shortcoming was the unexpected flame concentration on the drivetrain components. General charring and burning of the structural and drivetrain assemblies occurred due to this flame concentration, as observed in Fig. 14c, but did not have negative impacts, with the exception of the actuator; the burning caused significant damage to the actuator wires and slight damage to the main actuator electronics housing. As a result, improvements in both vane material and thermal protection system are required.



(a) JVA before static firing.

(b) JVA after static firing.

(c) Observed charring on the JVA.

Fig. 14 Impacts of motor burn on JVA during the static fire.

A. Vane Material & Geometry Reselection

Due to immediate erosion of the tungsten-copper alloy, refinement of the jet vane material and geometry are required. Further research into properties of the Aerotech N1000W motor reveals aluminum oxide particulates as the primary makeup of motor exhaust. Aluminum oxide has an approximate hardness of 9 on the Mohs scale; as a result, the vane

material must have at least an equivalent hardness to endure the flow regime for an extended period. The only feasible material option from a cost and manufacturing standpoint is near-pure tungsten, which also has a hardness of 9. This material selection makes manufacturing a driving constraint on vane design, and as a result, the vane geometry was made as simple as possible while retaining structural integrity.

The jet vane contour was redesigned to feature a double-wedge airfoil and a simpler mounting geometry for ease of manufacturing. The key-slot architecture was preserved but reversed, placing the key feature on the jet vane instead of the vane backing, as seen in Fig. 15. As tungsten is not manufacturable by the GNC team using available equipment, this redesign was also driven by budgetary constraints for outsourcing tungsten manufacturing.

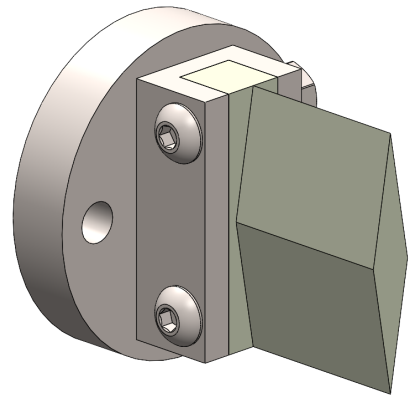


Fig. 15 Refined jet vane and vane backing geometries.

B. Thermal Protection System

In addition to jet vane erosion issues, significant heat flux opposite to the flow direction concentrated near the flange plate caused severe damage to actuator wires. To minimize this heat flow to actuators and improve electrical system shielding, a two-part TPS was developed. The first portion shields against aft ring convective radial heat transfer using a 3D-printed ablative sheath. The distance between the actuators and aft ring was maximized under the spatial constraint of the COTS airframe dimensions, and the 3D-printed sheath completely infills all remaining space in the vertical region of the actuator. This sheath provides a radial heat barrier between the aft ring and actuators, as exhibited in Fig. 16b. The material for this sheath was selected to be a carbon-fiber reinforced nylon composite filament, providing maximum heat resistance out of potential additive manufacturing material options.

The second portion protects against physical flame plumes in the reverse direction of the flow, which were observed during the static fire. These flames approach the drivetrain and actuator from directly above and are more concerning than radial heat due to their direct contact with components, requiring the implementation of heat-resistant materials. As such, a G10 (flame retardant) plate was designed to wedge between the actuator and drivetrain while resting above the 3D-printed portion of the TPS, covering the actuator and respective electrical pathways, visualized in Fig. 16b.

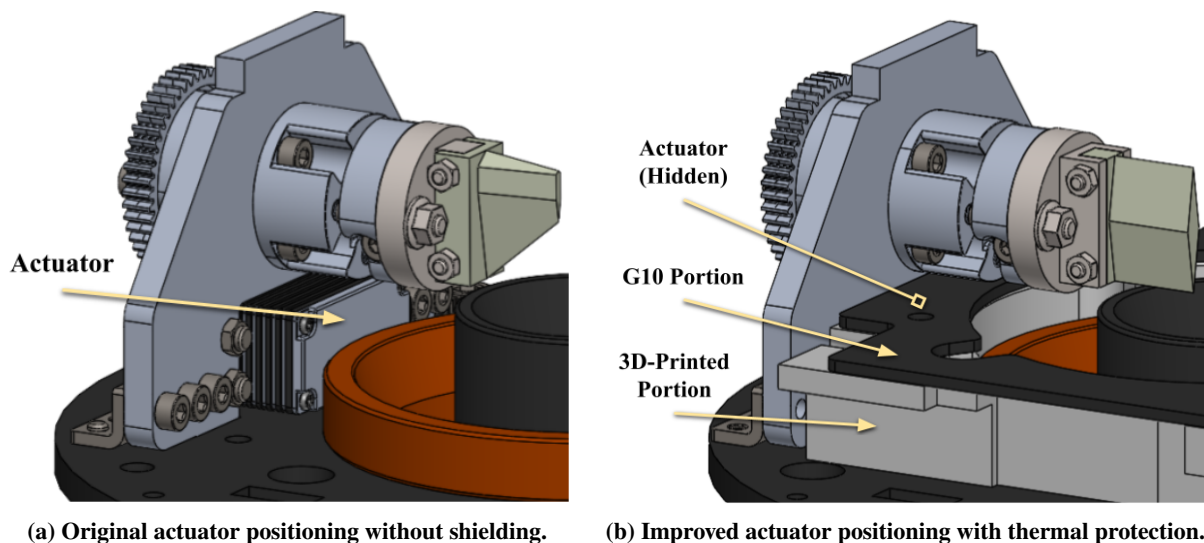
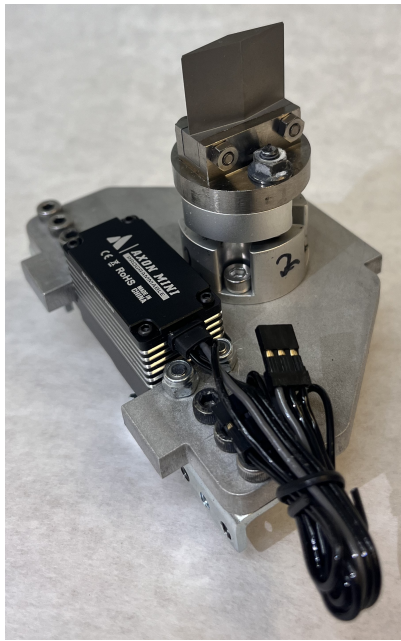


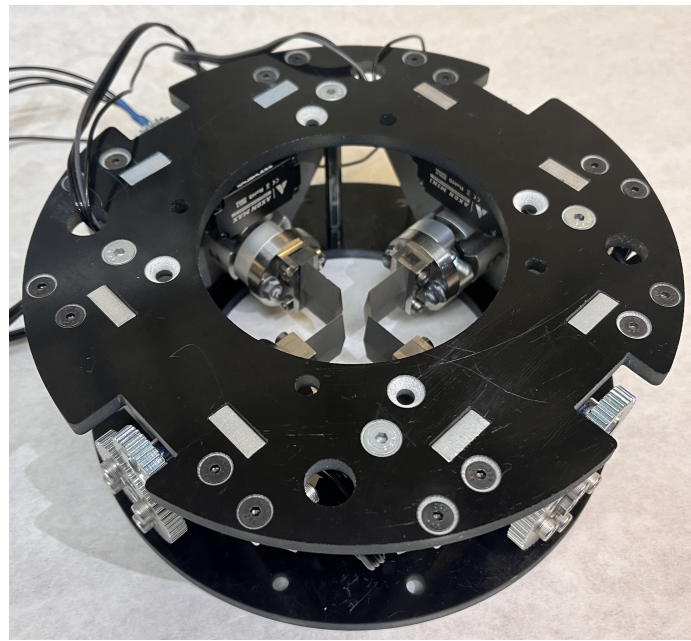
Fig. 16 Implementation of actuator thermal protection system.

C. Final Iteration Integration & Assembly

Implementing the post-static fire improvements yields the final JVA, prepared for a final static fire. The completed manufacturing and integration of a drivetrain subassembly is exhibited in Fig. 17a, with complete system assembly exhibited in Fig. 17b.



(a) JVA drivetrain.



(b) JVA integrated structural and drivetrain assemblies.

Fig. 17 Manufactured and assembled JVA prepared for final static fire.

VIII. Conclusion

In pursuit of active stabilization, the GNC Team has researched, developed, and tested jet vane thrust vector control technology. The core element of this technological progression is the evolution of the jet vanes assembly — the mechanical system responsible for jet vane control. The composition of this assembly began with a sandwich-design structural subassembly designed to balance rigidity, weight, and manufacturability. A two-stage jet vane drivetrain subassembly was integrated into the structural subassembly, coordinated to distance actuators from the flow regime, transfer actuator motion, and interface commercial off-the-shelf components. Initial feasibility calculations extending to finite element analysis verified the structural integrity of the subassemblies, leading to material selection optimization of system performance. Initial static fire tests validated the structure and drivetrain architectures but revealed critical issues with jet vane erosion and thermal exposure. In response, the jet vanes were upgraded to pure tungsten for increased hardness, and a thermal protection system was introduced to shield actuators from excessive heat. With these improvements, the JVA has been iterated, completely manufactured, and poised for final static fire verification before integration into a rocket for launch.

References

- [1] Gardner, S. R., “Erosion effects on TVC vane heat transfer characteristics,” Ph.D. thesis, Monterey, California. Naval Postgraduate School, 1994.
- [2] “Axon MINI+ Programmable Servo,” 2025. URL <https://axon-robotics.com/products/mini>.
- [3] W.H.Dornfeld, “Gear Tooth Strength Analysis,” 2006. URL <http://www.faculty.fairfield.edu/wdornfeld/ME312/ToothLoads04.pdf>.
- [4] Bauccio, M. E., *ASM Engineered Materials Reference Book*, 2nd ed., ASM International, Materials Park, OH, 1994.
- [5] Senkov, O., Dubois, M., and Jonas, J., “Elastic moduli of titanium-hydrogen alloys in the temperature range 20 C to 1100 C,” *Metallurgical and Materials Transactions A*, Vol. 27, 1996, pp. 3963–3970.
- [6] Ayoub, H., El-sherif, A. F., Hassan, H., and Khairy, S., “Young’s modulus of tungsten at elevated temperatures using synchronous laser shadow vibrometry,” *The International Conference on Mathematics and Engineering Physics*, Military Technical College, 2018, pp. 1–21.